Article ID: 1000-324X(2020)02-0224-07 **DOI:** 10.15541/jim20190112

Interfacial Stress Analysis on Skutterudite-based Thermoelectric Joints under Service Conditions

SHAO Xiao[1,2], LIU Rui-Heng[1,3], WANG Liang[1], CHU Jing[1,2], BAI Guang-Hui[4], BAI Sheng-Qiang[1,3], GU Ming[1], ZHANG Li-Na[4], MA Wei[4], CHEN Li-Dong[1,3]

(1. The State Key Lab of High Performance Ceramics and Superfine Microstructure, Shanghai Institute of Ceramics, Chinese Academy of Sciences, Shanghai 201899, China; 2. University of Chinese Academy of Sciences, Beijing 100049, China; 3. Center of Materials Science and Optoelectronics Engineering, University of Chinese Academy of Sciences, Beijing 100049, China; 4. Science and Technology on Space Physics Laboratory, Beijing 100076, China)

Abstract: In thermoelectric (TE) devices, the interfacial reliability greatly influenced devices' durability and power output. For skutterudites (SKD) devices, TE legs and electrodes are bonded together with diffusion barrier layer (DBL). At elevated temperatures, DBL react with SKD matrix or electrode to generate complex interfacial microstructures, which often accompanies evolutions of the thermal, electrical and mechanical properties at the interfaces. In this work, a finite element model containing the interfacial microstructure characteristics based on the experimental results was built to analyze the interfacial stress state in the skutterudite-based TE joints. A single-layer model was applied to screen out the most important parameters of the coefficient of thermal expansion (*CTE*) and the modulus of DBL on the first principle stress. The multilayer model considering the interfacial microstructures evolution was built to quantitively simulate the stress state of the TE joints at different aging temperatures and time. The simulation results show that the reactive $CoSb_2$ layer is the weakest layer in both SKD/Nb and SKD/Zr joints. And by prolonging the aging time, the thickness of the reaction layer continuously increased, leading to a significant raising of the interfacial stress. The tensile testing results of the SKD/Nb joints match the simulation results well, consolidating accuracy and feasibility of this multilayer model. This study provides an important guidance on the design of DBL to improve the TE joints' mechanical reliability, and a common method to precisely simulate the stress condition in other coating systems.

Key words: thermoelectric joints; diffusion barrier layer; finite element model; tensile strength

Thermoelectric (TE) technology has attracted great attention because it can convert heat into electric power directly with the advantages of no moving parts and long durability, especially for the applications in deep space exploration, waste heat recovery, and other special fields[1-3]. Over the past several decades, many high-performance TE materials and devices were developed[4-8], providing great opportunities for large-scale application of TE power generation. Among them, skutterudite-based (SKD) devices exhibited very high conversion efficiencies up to 12%[9], making SKD one of the most potential candidates for the practical applications.

As the SKD device steps forward to industrial application from laboratory[10], the mechanical reliability becomes the top concern since TE devices often work under harsh service conditions, such as high temperature difference, mechanical vibration with wide frequency, extremely long service time. A TE device comprises of n-, p-type TE legs and electrodes as major components. Previously, researchers paid a lot of attention to the mechanical property of SKD materials themselves[11-13], and demonstrated that the SKD materials exhibit excellent mechanical performance to bear service stress[14-15]. However, at the electrode interface, the Sb elements of skutterudites matrix diffused into electrode materials such as Cu, Ni, and Mo[16-17] or diffusion barrier layer (DBL) such as Ti, Mo, Mo-Ti, $Cr_{80}Si_{20}$, Nb, $Ti_{100-x}Al_x$ (x= 3–12)[18-23] during the long-time service at high temperatures. The elemental diffusions and chemical reactions at the interface not only result in dramatical increase of the

Received date: 2019-03-18; **Revised date:** 2019-04-30
Foundation item: National Key Research and Development Program of China (2018YFB0703600); National Natural Science Foundation of China (51572282, 51632010, 11572050); Youth Innovation Promotion Association CAS
Biography: SHAO Xiao (1995–), male, Master candidate. E-mail: shaoxiao@student.sic.ac.cn
邵 笑(1995–), 男, 硕士研究生. E-mail: shaoxiao@student.sic.ac.cn
Corresponding author: LIU Rui-Heng, associate professor. E-mail: liurh@mail.sic.ac.cn
刘睿恒, 副研究员, E-mail: liurh@mail.sic.ac.cn

interfacial electrical and thermal resistivity[24], but also induce the mechanical injury or disability.

Numerical analysis for residual interfacial stress in multilayer system was well studied in the past decades. It was recognized that the coefficient of thermal expansion (*CTE*) of the component layers plays a critical role on interfacial reliability[25]. Interface morphology should also affect interface stability in multilayer systems like thermal barrier coatings[26]. Li, *et al*[27] found that the thermal stress in segmented $CoSb_3$/Bi_2Te_3 device could be reduced by introducing a graded layer between $CoSb_3$ and copper electrode. However, all above researches treated multilayer systems as inert (without compositional or structural change) at high temperature. Actually, in TE joints, element diffusion and reaction are inevitable during whole service life. Therefore, the interfacial compositions and microstructures would continuously evolve, which influence the interfacial mechanical behavior unexpectedly.

This study reports a numerical analysis model based on finite element simulation method to investigate the dynamic interfacial stress at the SKD/DBL joint by taking the microstructure evolution into account. A single-layer model was established, and the interfacial stress in the TE joints with different DBL was calculated. Based on the experimental results on the interface observation and properties measuring of reaction layers, a multilayer model considering microstructure evolution was built to quantitively simulate the stress state of the aged TE joints. The tensile test results of SKD/Nb joints matched well with the simulation results.

1 Finite element model and experimental procedure

1.1 Governing equation of thermal-structural model

A transient thermal-structural model is applied for stress in SKD/DBL joints to simulate the sintering-cooling process. Residual stress results from change of temperature and difference of material properties. For cooling period, the transient thermal conducting equation can be derived according to energy conservation law:

$$\rho C_p \frac{\partial T}{\partial t} + \nabla \cdot \boldsymbol{q} = \dot{q} \tag{1}$$

$$\boldsymbol{q} = -[\kappa] \cdot \nabla T \tag{2}$$

Where T is absolute temperature, ρ is the density, C_p is isobaric heat capacity, $\boldsymbol{q}$ is the heat flux vector, $\dot{q}$ is heat generation rate, $[\kappa]$ stands for thermal conductivity matrix dependent with T. From Eq. (1–2), the temperature distribution in model can be worked out.

Once temperature decreases, the difference between *CTE* of SKD and Nb causes displacement, which can be converted to strain, and then results in stress according to generalized Hooke's law. Thus the thermal-structural governing equation can be expressed as[28]:

$$\boldsymbol{\sigma} = [D]\boldsymbol{\varepsilon} - [D]\boldsymbol{\alpha} \cdot T \tag{3}$$

Where $\boldsymbol{\sigma}$ and $\boldsymbol{\varepsilon}$ are stress and strain vectors respectively, $[D]$ is stiffness matrix, $\boldsymbol{\alpha}$ is *CTE* vector, ΔT is the difference between present temperature and reference temperature (T_0). Finally, the stress distribution can be figured out.

For a certain site in materials, stress tensor can be divided to three principle stresses: $\boldsymbol{\sigma_1}$, $\boldsymbol{\sigma_2}$, $\boldsymbol{\sigma_3}$, from large to small, respectively. According to the first strength theory, the maximum principle stress is the main reason for fracture, which coincides well with the fracture of brittle materials' uniaxial tension. Therefore, the first principle stress σ_1 is chosen to evaluate stress intensity.

In initial state (t=0), adjacent materials are already bonded closely to form a zero-stress state. Thus, the initial temperature (960 K) is reference temperature (T_0) of thermal expansion. Then in cooling process, joint's diameter is assumed to be unchanged, meanwhile upper and lower end could move vertically. Besides, model's round side is considered as thermal insulated. On the end side surfaces, effect of cooling is also simplified as natural convection in air, in which the heat transfer coefficient was set to be 10 $W \cdot m^2 \cdot K^{-1}$.

1.2 Experimental procedures

SKD/Nb joints were fabricated and aged for tensile test. $Yb_{0.3}Co_4Sb_{12}$ (SKD) powders and Nb foil ((0.025± 0.015) mm) were loaded into a graphite die with a diameter of 50 mm, and then sintered by hot pressed for 90 min at 690 ℃ and 60 MPa under Ar atmosphere. Nb foil was placed between two SKD layers to form a sandwich structure. The obtained joint (ϕ50 mm×4 mm) was then cut into small cylinders (ϕ10 mm) and sealed in quartz ampules under vacuum. The sealed ampules were aged under 600 and 650 ℃ in furnace for various time, and the aged joints were denoted as "temperature-aging time", such as 600–10 d. The tensile strength was measured by Instron-5566 universal testing system at room temperature. The microstructures of interface and fracture surface were observed by SEM (ZEISS Spura 55). The constituents of interface were measured by EDS (Oxford Instrument).

2 Results and discussion

2.1 Influence of materials properties in single-layer model

Nb, Mo, Zr, Ti were chosen as the DBL candidates for SKD[22,29]. The effect of materials properties on interfa-

cial mechanical stability was studied by using single-layer model. The *CTE* and Young's modulus data obtained from COMSOL database are presented in Fig. 1(a-b). The calculated σ_1 are shown in Fig. 1(c). Compared with other DBL materials, the stress intensity of SKD/Mo is extremely high, which probably results from great difference of *CTE* between Mo and SKD (*CTE*=10.6×10^{-6} K^{-1}[20]). The stress of SKD/Zr interface is the lowest (1.1 GPa), even though Zr has the larger difference of *CTE* with SKD than that of Ti. Fig. 1(c) shows that the variation trend of interfacial stress is the same as that of Young's modulus. It is observed that both *CTE* and Young's modulus influence stress intensity, and large Young's modulus induces high intensity stress. Moreover, in single-layer model, the thickness of DBL affects interfacial stress weakly. In consideration of reaction activity at high temperature[22], Nb and Zr are employed for further research.

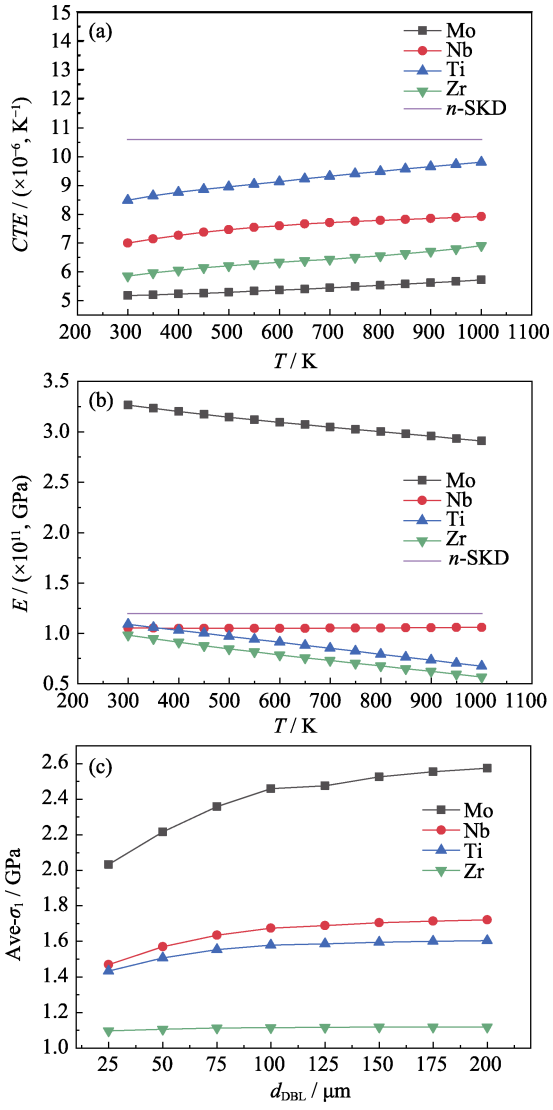

Fig. 1 (a) *CTE*, (b) Young's modulus (*E*), and (c) variations of average first principle stresses with thicknesses of different DBL candidates (purple lines: *CTE* and *E* of SKD)

2.2 Influence of thickness of layers in multi-layer model

Actually, all the SKD joints undergo the elemental diffusion and chemical reaction during long-time service at high temperature[8], which makes single-layer model inaccurate to describe the stress state of aged joints. SEM and EDS results of SKD/Nb joints after different aging time are listed in Fig. A2. No evident microcracks or micropores are observed in as-prepared joint. After aged at 600 ℃ for 5 d, $NbSb_2$ and $CoSb_2$ are detected, and micropores appear in the $CoSb_2$ layer. The thickness of $NbSb_2$ slightly increase with the increase of aging time (Fig. A2(b-d)), indicating that elevating temperature and prolonging aging time significantly aggravate diffusion and reaction. The reaction process can be described as following. At the initial stage of aging, SKD didn't react with DBL, and there are only three layers, as the single-layer model is shown in Fig. 2(a). With aging accelerating, SKD reacted with Nb to form $CoSb_2$ and $NbSb_2$, and micropores appeared simultaneously because of the volume change. The reaction equation can be expressed in Eq. (4):

$$2CoSb_3 + Nb \rightarrow 2CoSb_2 + NbSb_2 \quad (4)$$

Thus, multilayer model was built to find out the influence of micropores and diffusion layers.

To simplify the modeling and calculation, there're some requisite assumptions in the model: (1) $CoSb_2$ and $NbSb_2$ layers are assumed to be totally flat; (2) Micropores are of ellipsoid shape, in which *x* and *y* semi-major axis (*a* and *b*) are equal to a multiple of *z* semi-major axis (*c*); (3) Micropores locate on the interface between $NbSb_2$ and $CoSb_2$ periodically; (4) Diameter of cylindrical

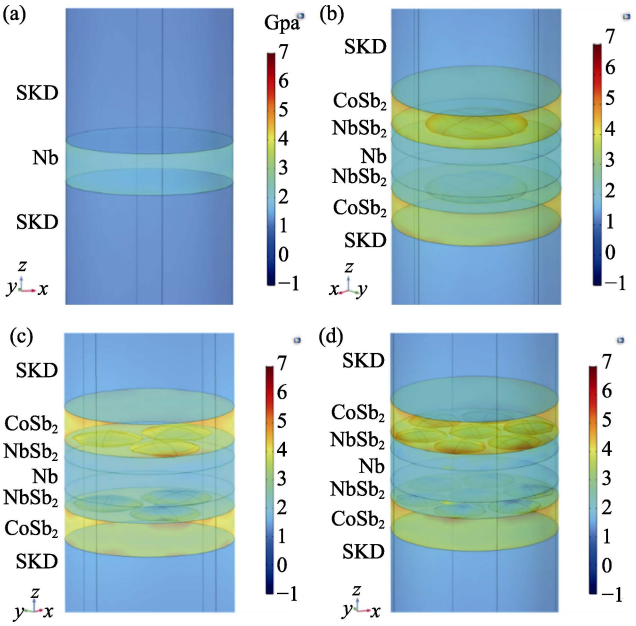

Fig. 2 σ_1 distributions for (a) *n*=0, (b) *n*=1, (c) *n*=3, and (d) *n*=7 (initial thickness of Nb: 25 μm)

model is reduced; (5) Materials are seen as isotropic and completely linear-elastic; (6) Part of material properties (Table A1) is treated as constant value or simple function of temperature because of lack in experimental data. Combining materials' molar mass and density listed in Table A1, relationships of thickness of each layer can be obtained, as shown in Table 1. Thus, total volume of micropores ought to equal the volume difference between models before and after aging. Therefore, the relationship (Eq. (5)) between average micropore size and thickness of $NbSb_2$ is listed:

$$c=\left(\frac{3r^2 d_{\mathrm{NbSb_2}}\cdot\Delta V}{4m^2 n}\right)^{\frac{1}{3}} \tag{5}$$

Where r is radius of model, d_{NbSb2} is thickness of $NbSb_2$, ΔV is total volume of micropores, m is the ratio of a (or b) to c, n is number of micropores at given total micropore volume. As long as micropores' shape, numbers and positions are certain, $d_{\mathrm{NbSb_2}}$ is expected to decide the extent of aging. Micropores' positions are considered to uniformly distribute at the $CoSb_2/NbSb_2$ interface. The number of micropores n was set as 1, 3, 7, and the distributions for each number are shown in Fig. 2(b-d). According to calculation results presented in Fig. A3, the ratio of a (or b) to c (m) made little difference to stress distribution, which won't be discussed in the next part.

The diffusion and reaction process of SKD/Zr joint is similar with SKD/Nb, and the reaction layer is $ZrSb_2$[22]. It can also be analyzed by using multilayer model, and the results are shown in Fig. A4.

The evolution of the interface can be simplified descripted by 3 parameters of n, d_{DBL} and $d_{\mathrm{NbSb_2}}$. The positions of micropores need to be set manually for each different n. When n changes from 1 to 7, the micropore size decreases from 5.3 μm to 1.2 μm. Furthermore, to eliminate the influence of abnormal stress caused by low-quality elements mesh in much thinner barrier layer and diffusion layer, average first principle stress is applied to evaluate interfacial stress intensity. Fig. 2(a) gives the initial stress distribution of SKD/Nb interface which is the same with the single layer model. The stress concentrates on Nb layer, and the maximum principle stresses of Nb/SKD interface is 2.383 and 1.46 GPa, respectively. Fig. 2(b-d) shows the σ_1 distribution in multilayer model with different micropore numbers n at the same given ΔV. After aging, all stress values with increasing n are much higher than the initial ones. For all cases, maximum stresses are found at the $CoSb_2$ layers. When $d_{\mathrm{NbSb_2}}$=10 μm, the maximum σ_1 are 5.83 GPa for n=1 and 7.79 GPa for n=7, indicating that the diffusion reaction induce large internal stress. Fig. 3 shows the d_{DBL} and $d_{\mathrm{NbSb_2}}$ dependent σ_1 at SKD/$CoSb_2$ and $CoSb_2/NbSb_2$ interfaces. The average stress of $CoSb_2/NbSb_2$ interface is always the largest value for different n, indicating that $CoSb_2/NbSb_2$ is the most unstable interface. In Fig. 3(b, e, h), contour lines are approximately parallel to d_{DBL} axis, which means the thickness of reactive $NbSb_2$ plays a dominate role on stress of $CoSb_2/NbSb_2$ interface.

Table 1　Relative volume changes for one interface (SKD/Nb and SKD/Zr joints)

Layer	SKD	Nb/Zr	$CoSb_2$	$NbSb_2$/$ZrSb_2$	Difference
Relative volume change (SKD/Nb)	–2.75	–0.27	+1.78	+1	–0.24
Relative volume change (SKD/Zr)	–2.48	–0.32	+1.65	+1	–0.15

2.3　Tensile test results and validation of models

SKD/Nb joints are fabricated and aged for tensile test. After fracture, bonding strength are calculated by Eq. (6):

$$\sigma_{\mathrm{t}}=\frac{F_{\max}}{A} \tag{6}$$

Where σ_{t} is tensile strength, $F_{\max}$ is the maximum load, A is base area of joints. The results are listed in Table 2. It is obvious that accelerated aging worsens interfacial bonding severely. With the $d_{\mathrm{NbSb_2}}$ grows from 0 to 12 μm, the tensile strength decreases from 9.68 MPa to 1.46 MPa. The decreasing trend of tensile strength is consistent with the increasing trend of calculated stress. Furthermore, after tension, by comparing structures and compositions of the fracture surfaces, location of the weakest interface can be found. All of the aged joints break at $CoSb_2$ layer (Fig. 4(d-e)), while the unaged joints break at SKD/Nb interface (Fig. 4(a)). With elevated aging temperature or prolonged aging time, the proportions of $CoSb_2$ on fracture surface (SKD side, Fig. 4(d)) increases obviously (Table 2), indicating that the fracture locations tend to be the $CoSb_2/NbSb_2$ interface. The fracture locations are completely consistent with calculation results. All of the experimental results verify the validity of above simulation model.

4　Conclusion

In this study, a single-layer model was established to calculate the interfacial stress in the TE joints with different DBL. It's found that the DBL materials with small modulus and similar *CTE* with SKD can reduce the interfacial stress. Based on the experimental results, a multilayer model considering microstructure evolution is built to quantitively simulate the stress state of the aged TE joints. Large thickness of reaction layers and volume changes can intensify stress at interface remarkably. Both in SKD/Zr and SKD/Nb joints, the biggest first principle stress locates at $CoSb_2$ layer. Tensile test results of SKD/

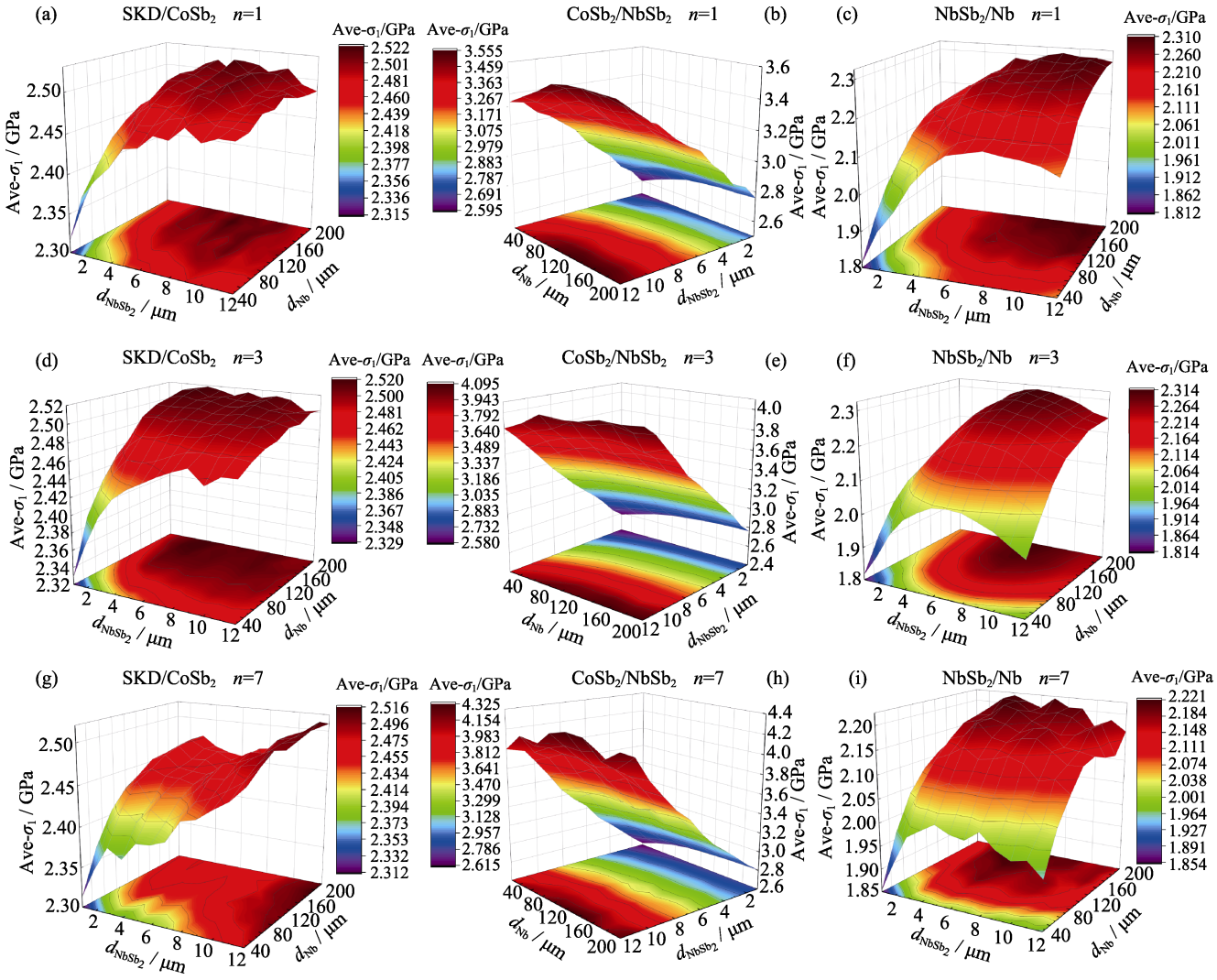

Fig. 3 Variations of average σ_1 on each interface with thicknesses of $NbSb_2$ and Nb

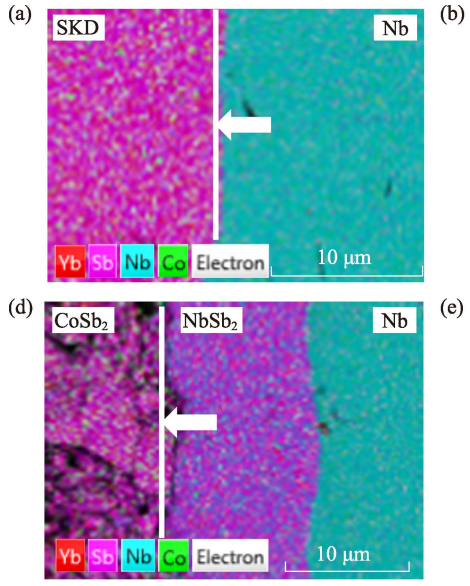

(c)

Element	at%
Co	24.57
Sb	73.01
Yb	2.43
Total	100.00

(f)

Element	at%
Co	31.53
Nb	0.55
Sb	66.46
Yb	1.46
Total	100.00

Fig. 4 EDS mappings of (a, d) interfaces and (b, e) fracture surfaces of (a-b) unaged joint and (d-e) sample 650-10d (White line indicating the fracture surface, and white arrow indicating direction of observation in (b) or (d)); Total element data were shown in table (c) for figure (b) and in table (f) for figure (e)

Table 2　Thicknesses of $NbSb_2$ layer d_{NbSb_2}, average sizes of micropores c, tensile strengths σ_t, maximum calculated stresses Ave-σ_1 and the location interfaces, compositions of tensile fracture surface for series of aging SKD/Nb joints

Joints	d_{NbSb_2}/μm	c/μm	n	Ave-σ_1/GPa	σ_t/MPa	Fracture position	Fracture composition
0 d	0	0	0	1.46	(9.68±1.70)	Nb/ SKD	(Nb+ $NbSb_2$)/(3%$CoSb_2$+97% SKD)
600–5 d	2	2.02	3	2.72	(4.63±2.12)	$CoSb_2$/$NbSb_2$	$NbSb_2$/(36%$CoSb_2$+64% SKD)
600–10 d	3	2.21	3	2.80	(3.39±1.44)	$CoSb_2$/$NbSb_2$	$NbSb_2$/(47%$CoSb_2$+53% SKD)
650–5 d	7	4.13	1	3.07	(4.44±1.50)	$CoSb_2$/$NbSb_2$	$NbSb_2$/(80%$CoSb_2$+20% SKD)
650–10 d	12	5.20	1	3.42	(1.46±0.38)	$CoSb_2$/$NbSb_2$	$NbSb_2$/(97%$CoSb_2$+3% SKD)

Nb joints fit simulation results well, proving the feasibility of this model to simulate the stress state in multilayer system containing complex microstructures, which is helpful to design the high stability electrode interface structure for SKD TE devices.

Supporting materials:

Supporting materials related to this article can be found at https://doi.org/10.15541/jim20190112.

References:

[1] BELL L E. Cooling, heating, generating power and recovering waste heat with thermoelectric systems. *Science*, 2008, **321(5895):** 1457–1461.

[2] CHAMPIER D. Thermoelectric generators: a review of applications. *Energy Conversion and Management*, 2017, **140:** 167–181.

[3] CHEN L, BAI S, ZHANG Q. Technologies and applications of thermoelectric devices: current status, challenges and prospects. *Journal of Inorganic Materials*, 2019, **34(3):** 279.

[4] SALES B C, MANDRUS D, WILLIAMS R K. Filled skutterudite antimonides: a new class of thermoelectric materials. *Science*, 1996, **272:** 1325–1328.

[5] LIU H, SHI X, XU F, *et al.* Copper ion liquid-like thermoelectrics. *Nature Materials*, 2012, **11(5):** 422–425.

[6] ZHAO L D, LO S H, ZHANG Y, *et al.* Ultralow thermal conductivity and high thermoelectric figure of merit in SnSe crystals. *Nature*, 2014, **508(7496):** 373–377.

[7] ZHANG Q H, HUANG X Y, BAI S Q, *et al.* Thermoelectric devices for power generation: recent progress and future challenges. *Advanced Engineering Materials*, 2016, **18(2):** 194–213.

[8] HE R, SCHIERNING G, NIELSCH K. Thermoelectric devices: a review of devices, architectures, and contact optimization. *Advanced Materials Technologies*, 2018, **3(4):** 1700256.

[9] ZHANG Q, LIAO J, TANG Y, *et al.* Realizing a thermoelectric conversion efficiency of 12% in bismuth telluride/skutterudite segmented modules through full-parameter optimization and energy-loss minimized integration. *Energy Environ. Sci.*, 2017, **10(4):** 956–963.

[10] YAO Z, QIU P, LI X, *et al.* Investigation on quick fabrication of n-type filled skutterudites. *Journal of Inorganic Materials*, 2016, **31(12):** 1375–1382.

[11] RAVI V, FIRDOSY S, CAILLAT T, *et al.* Mechanical properties of thermoelectric skutterudites. *AIP Conference Proceedings*, 2008, **969:** 656–662.

[12] SALVADOR J R, YANG J, SHI X, *et al.* Transport and mechanical properties of Yb-filled skutterudites. *Philosophical Magazine*, 2009, **89(19):** 1517–1534.

[13] DAHAL T, KIM H S, GAHLAWAT S, *et al.* Transport and mechanical properties of the double-filled p-type skutterudites $La_{0.68}Ce_{0.22}Fe_{4-x}Co_xSb_{12}$. *Acta Materialia*, 2016, **117:** 13–22.

[14] RUAN Z, LIU L, ZHAI P, *et al.* Residual strength degradation of $CoSb_3$ skutterudite compounds under low-cycle fatigue loading. *Journal of Electronic Materials*, 2012, **41(6):** 1487–1492.

[15] WEN P, ZHU Y, CHEN J, *et al.* The microstructure and thermoelectric properties of Yb-filled skutterudite $Yb_{0.1}Co_4Sb_{12}$ under cyclic thermal loading. *Journal of Materials Engineering and Performance*, 2016, **25(11):** 4764–4768.

[16] ZHAO D, LI X, HE L, *et al.* Interfacial evolution behavior and reliability evaluation of $CoSb_{(3)}$/Ti/Mo-Cu thermoelectric joints during accelerated thermal aging. *Journal of Alloys and Compounds*, 2009, **477(1/2):** 425–431.

[17] SHI L, HUANG X, GU M, *et al.* Interfacial structure and stability in Ni/SKD/Ti/Ni skutterudite thermoelements. *Surface and Coatings Technology*, 2016, **285:** 312–317.

[18] FAN X C, GU M, SHI X, *et al.* Fabrication and reliability evaluation of $Yb_{0.3}Co_4Sb_{12}$/Mo–Ti/Mo–Cu/Ni thermoelectric joints. *Ceramics International*, 2015, **41(6):** 7590–7595.

[19] WOJCIECHOWSKI K T, ZYBALA R, MANIA R. High temperature $CoSb_3$–Cu junctions. *Microelectronics Reliability*, 2011, **51(7):** 1198–1202.

[20] GU M, XIA X, LI X, *et al.* Microstructural evolution of the interfacial layer in the Ti–Al/$Yb_{0.6}Co_4Sb_{12}$ thermoelectric joints at high temperature. *Journal of Alloys and Compounds*, 2014, **610:** 665–670.

[21] TANG Y S, BAI S Q, REN D D, *et al.* Interface structure and electrical property of $Yb_{0.3}Co_4Sb_{12}$/Mo-Cu element prepared by welding using Ag-Cu-Zn solder. *Journal of Inorganic Materials*, 2015, **30(3):** 256–260.

[22] GU M, BAI S, WU J, *et al.* A high throughput strategy to screen interfacial diffusion barrier materials for thermoelectric modules. *Journal of Materials Research*, 2019, **34(7):** 1179–1187.

[23] CHEN L, BAI S, LIU R, *et al.* Interface stability of skutterudite thermoelectric materials/$Ti_{88}Al_{12}$. *Journal of Inorganic Materials*, 2018, **33(8):** 889–894.

[24] EL-GENK M S, SABER H H, CAILLAT T, *et al.* Tests results and performance comparisons of coated and un-coated skutterudite based segmented unicouples. *Energy Conversion and Management*, 2006, **47(2):** 174–200.

[25] HSUEH C H. Thermal stresses in elastic multilayer systems. *Thin Solid Films*, 2002, **418:** 182–188.

[26] HAN M, HUANG J, CHEN S. The influence of interface morphology on the stress distribution in double-ceramic-layer thermal barrier coatings. *Ceramics International*, 2015, **41(3):** 4312–4325.

[27] LI Y, YANG X Q, ZHAI P C, *et al.* Thermal stress simulation and optimum design of $CoSb_3$/Bi_2Te_3 thermoelectric unicouples with graded interlayers. *AIP Conference Proceedings*, 2008, **973:** 297–302.

[28] JIA X, GAO Y. Estimation of thermoelectric and mechanical per-

formances of segmented thermoelectric generators under optimal operating conditions. *Applied Thermal Engineering*, 2014, **73(1):** 335–342.

[29] GU M, XIA X, HUANG X, *et al.* Study on the interfacial stability of p-type Ti/$Ce_yFe_xCo_{4-x}Sb_{12}$ thermoelectric joints at high temperature. *Journal of Alloys and Compounds*, 2016, **671:** 238–244.

服役条件下方钴矿基热电元件的界面应力分析

邵 笑[1,2], 刘睿恒[1,3], 王 亮[1], 初 靖[1,2], 白光辉[4],
柏胜强[1,3], 顾 明[1], 张丽娜[4], 马 伟[4], 陈立东[1,3]

(1. 中国科学院 上海硅酸盐研究所, 高性能陶瓷和超微结构国家重点实验室, 上海 201899; 2. 中国科学院大学, 北京 100049; 3. 中国科学院大学 材料科学与光电技术学院, 北京 100049; 4. 空间物理重点实验室, 北京, 100076)

摘 要: 热电器件中, 界面可靠性是影响整体稳定和功率输出的关键因素。对于方钴矿(SKD)器件, 热电臂和电极通过扩散阻挡层(DBL)连接。在高温下, DBL 与 SKD、电极之间会发生反应并生成复杂的界面结构, 导致界面附近的热、电、力学性能发生变化。本研究根据实际界面结构建立了包含微观结构的有限元模型, 并将其用于分析方钴矿基元件的界面应力状态。采用单层模型对 DBL 材料参数进行了筛选, 发现热膨胀系数(*CTE*)和弹性模量(*E*)对第一主应力有显著影响。采用包含界面微结构的多层模型定量模拟了不同老化温度、时间下元件内部的应力分布, 结果表明在 SKD/Zr 和 SKD/Nb 中, $CoSb_2$ 反应层最为薄弱, 随着老化时间的延长, 反应层的厚度增加, 界面应力变大。同时, 元件的拉伸试验结果与计算结果吻合较好, 验证了模型的准确性与可行性。本研究为提升 SKD/DBL 元件的结构稳定性提供了指导, 同时也为精确模拟多层结构中的应力状态提供了研究思路。

关 键 词: 热电元件; 扩散阻挡层; 有限元模型; 拉伸强度

中图分类号: TQ174 **文献标识码:** A

Supporting information:

Interfacial Stress Analysis on Skutterudite-based Thermoelectric Joints under Service Conditions

SHAO Xiao[1,2], LIU Rui-Heng[1,3], WANG Liang[1], CHU Jing[1,2], BAI Guang-Hui[4], BAI Sheng-Qiang[1,3], GU Ming[1], ZHANG Li-Na[4], MA Wei[4], CHEN Li-Dong[1,3]

(1. The State Key Lab of High Performance Ceramics and Superfine Microstructure, Shanghai Institute of Ceramics, Chinese Academy of Sciences, Shanghai 201899, China; 2. University of Chinese Academy of Sciences, Beijing 100049, China; 3. Center of Materials Science and Optoelectronics Engineering, University of Chinese Academy of Sciences, Beijing 100049, China; 4. Science and Technology on Space Physics Laboratory, Beijing 100076, China)

Table A1　Basic properties including molar mass, density, Young's modulus, Poisson's ratio, thermal conductivity, thermal expansions and heat capacity for series of materials

Material	SKD	$CoSb_2$	$NbSb_2$[1]	$ZrSb_2$[2]	Nb	Zr
Molar Mass/(g·mol^{-1})	424.21	302.45	336.43	334.82	92.91	91.22
Density/(g·cm^{-3})	7.80*	8.36	8.29	7.62	8.57–8.45	6.5–6.4
Young's modulus/GPa	120*	160	186.1	135.7	104.8–105.7	97–57
Poisson's ratio	0.21[3]	0.23	0.21	0.243	0.382–0.394	0.34
Thermal conductivity/(W·m^{-1}·K^{-1})	3.04–4.05*	6.8–12.5[4]	24	10	55–65	20–25
Thermal expansion/(×10^{-6}, K^{-1})	10–11[5]	14–23[6]	8.4	9.7	7–7.8	5.9–6.9
Heat capacity/(J·g^{-1}·K^{-1})	0.22–0.23*	0.247	0.222	0.223	0.27–0.45	0.28–0.34

* Properties of Nb and Zr come from COMSOL' s materials database; Heat capacity of $CoSb_2$ and $NbSb_2$ are calculated by Dulong-Petit law; Data of SKD are obtained by previous experimental results

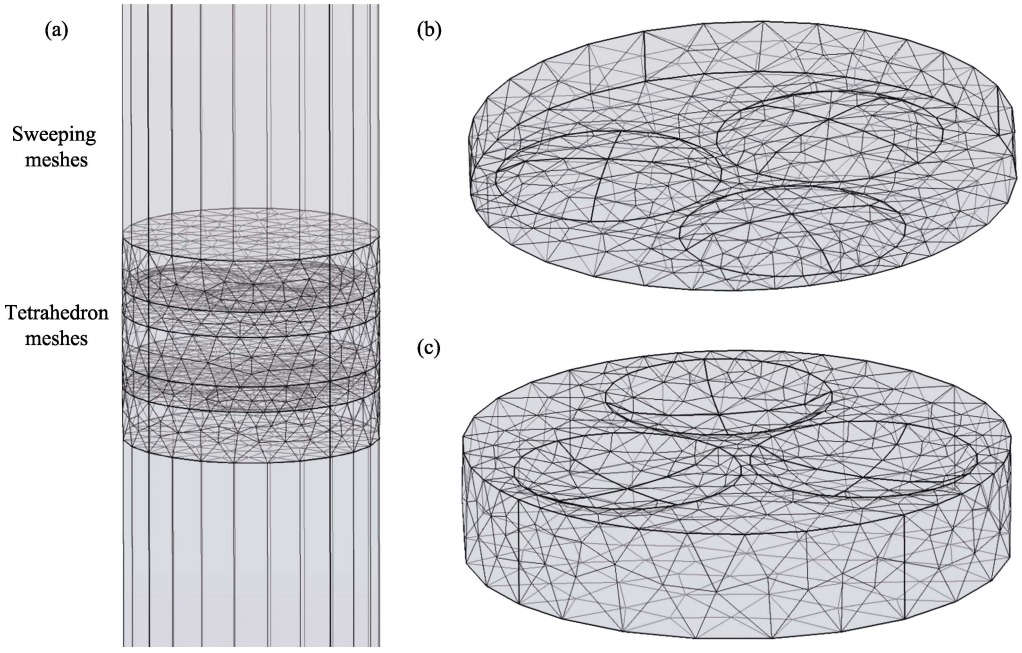

Fig. A1　(a) Finite element model of SKD/Nb joint with pores, detailed meshes of (b) $NbSb_2$ layer and (c) $CoSb_2$ layer

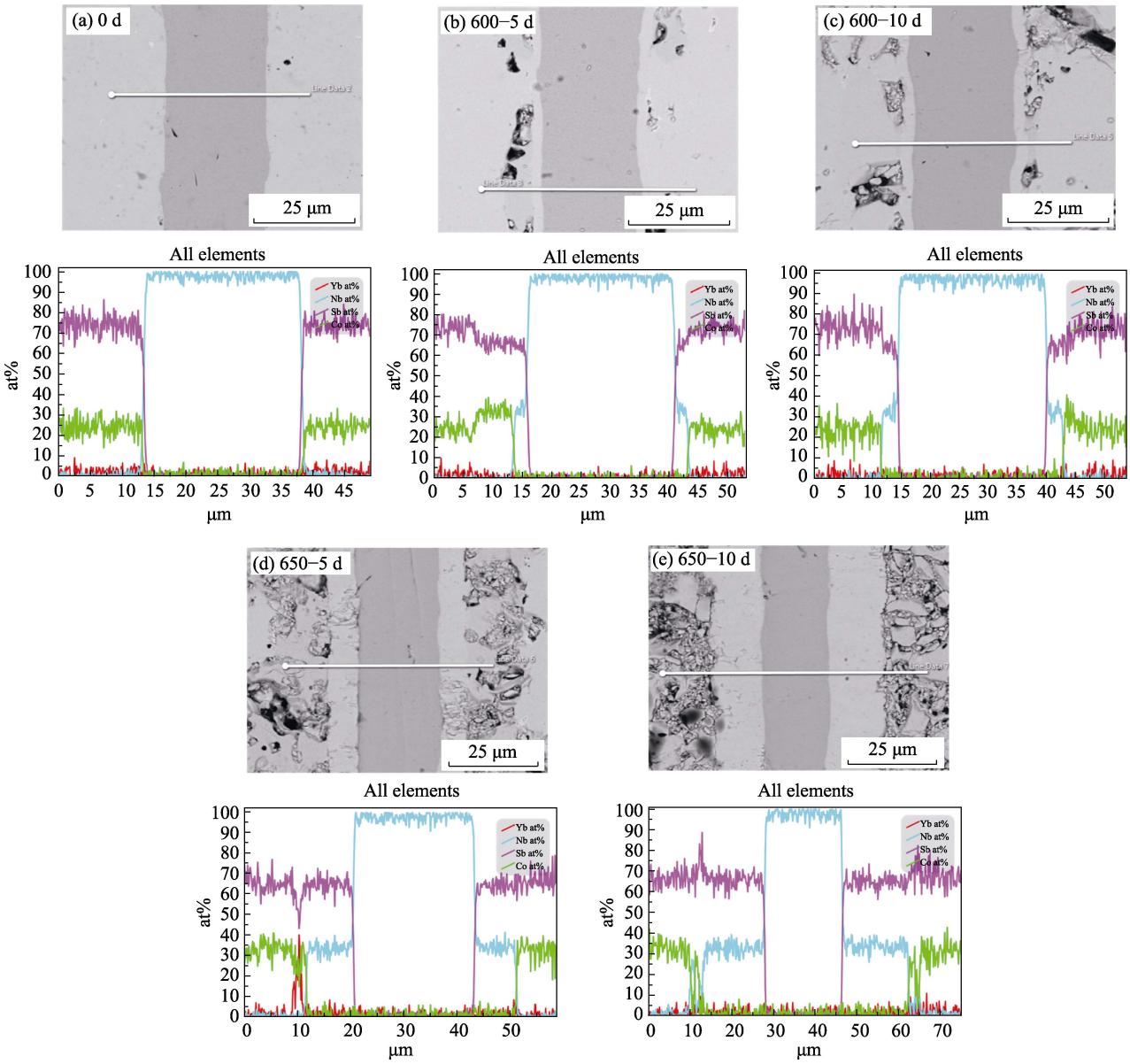

Fig. A2 Interface structures and line scans of joints

(a) As-prepared; (b) Aged at 600 ℃ for 5 d; (c) Aged at 600 ℃ for 10 d; (d) Aged at 650 ℃ for 5 d; (e) Aged at 650 ℃ for 10 d

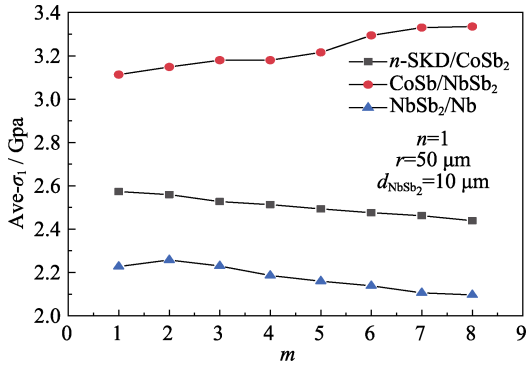

Fig. A3 Relationships between interface stresses and pores major axis ratios

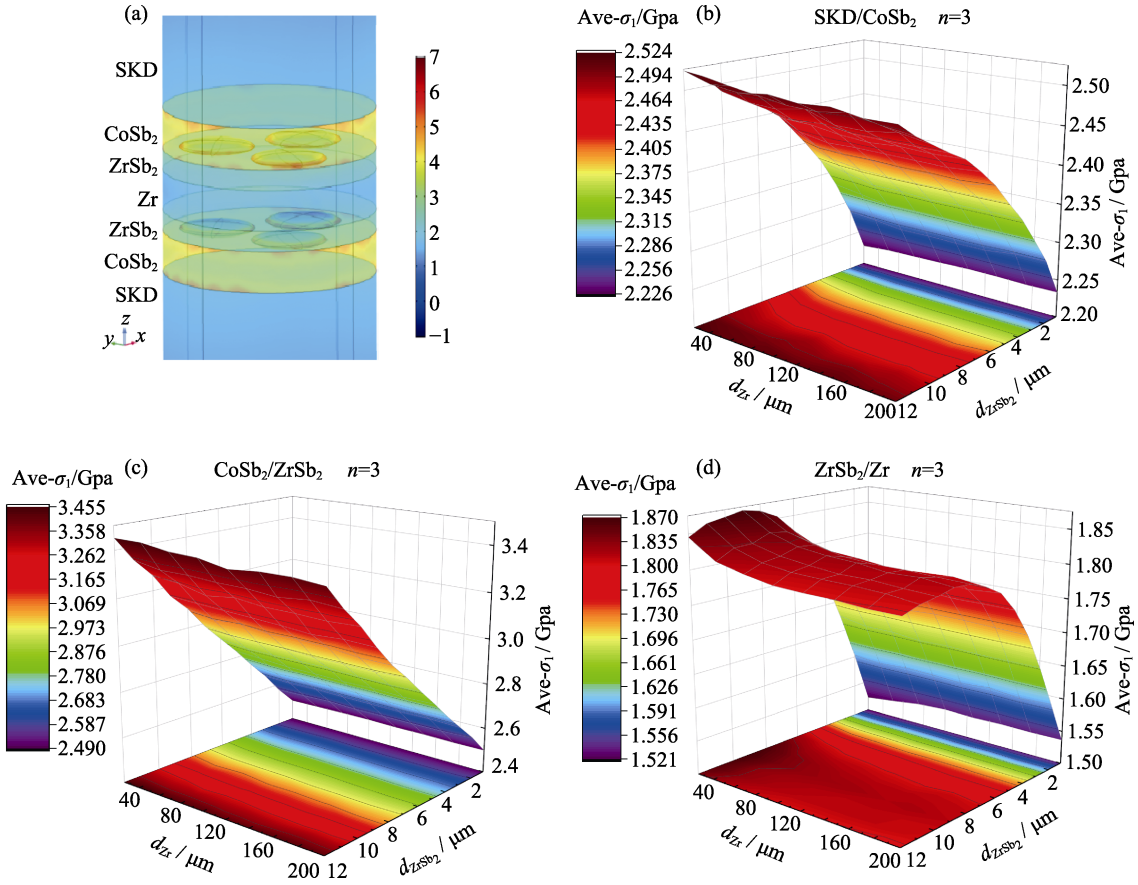

Fig. A4　(a) Calculated stress state of SKD/Zr joint with the Zr layer of 25 μm and the micropores number *n* of 3; (b) Variation of average σ_1 on SKD/$CoSb_2$ interface with thickness of $ZrSb_2$ and Zr (*n*=3); (c) Variation of average σ_1 on $CoSb_2$/$ZrSb_2$ interface with thickness of $ZrSb_2$ and Zr (*n*=3); (d) Variation of average σ_1 on $ZrSb_2$/Zr interface with thickness of $ZrSb_2$ and Zr (*n*=3)

参考文献:

[1] FAILAMANI F, BROZ P, MACCIÒ D, *et al.* Constitution of the systems {V,Nb,Ta}-Sb and physical properties of di-antimonides {V,Nb,Ta}Sb_2. *Intermetallics*, 2015, **65:** 94–110.

[2] TAVASSOLI A, GRYTSIV A, FAILAMANI F, *et al.* Constitution of the binary M-Sb systems (M=Ti, Zr, Hf) and physical properties of MSb_2. *Intermetallics*, 2018, **94:** 119–132.

[3] SALVADOR J R, YANG J, SHI X, *et al.* Transport and mechanical properties of Yb-filled skutterudites. *Philosophical Magazine*, 2009, **89(19):** 1517-1534.

[4] GOTO Y, MIYAO S, KAMIHARA Y, *et al.* Electrical/thermal transport and electronic structure of the binary cobalt pnictides $CoPn_2$ (Pn=As and Sb). *AIP Advances*, 2015, **5(6):** 067147.

[5] ZHAO D, LI X, JIANG W, *et al.* Fabrication of $CoSb_3$/MoCu thermoelectric joint by one-step SPS and evaluation. *Journal of Inorganic Materials*, 2009, **24(3):** 545–548.

[6] BÖRNSTEIN L. $CoSb_2$: Crystal Structure, Physical Properties, in: Madelung U R O, Schulz M (Ed.), Non-tetrahedrally Bonded Binary Compounds ii. Berlin: Springer-Verlag, 2000.